Mixing Behavior of Symmetric Chain Length and Mixed Chain Length Phosphatidylcholines in Two-Component Multilamellar Bilayers: Evidence for Gel and Liquid-Crystalline Phase Immiscibility†

Jeffrey T. Mason*

Department of Biochemistry, University of Virginia School of Medicine, Charlottesville, Virginia 22908

Received July 20, 1987; Revised Manuscript Received February 10, 1988

ABSTRACT: The mixing behavior of symmetric chain length and mixed chain length phosphatidylcholines in two-component multilamellar bilayers has been investigated by high-sensitivity differential scanning calorimetry. Phase diagrams have been constructed for two-component bilayers composed of C(18)C(18)PC and either C(18)C(16)PC, C(18)C(14)PC, C(18)C(12)PC, or C(18)C(10)PC. It is found that C(18)C(18)PC–C(18)C(16)PC and C(18)C(18)PC–C(18)C(14)PC mixed bilayers exhibit complete miscibility of the components in both the gel and liquid-crystalline phases. Whereas this mixing is observed to be nearly ideal for the C(18)C(18)PC–C(18)C(16)PC binary system, the intermixing of the lipids is highly nonideal in the gel phase of the C(18)C(18)PC–C(18)C(14)PC binary mixture. The C(18)C(18)PC–C(18)C(12)PC and C(18)C(18)PC–C(18)C(10)PC mixed bilayers are characterized by partial immiscibility of the phosphatidylcholine components in the bilayer gel phase. Over a large compositional range, these bilayers appear to consist of phase-separated regions of interdigitated and noninterdigitated gel phases. In addition, the C(18)C(18)PC–C(18)C(10)PC two-component bilayer displays a limited region of liquid–liquid immiscibility in the liquid-crystalline bilayer phase. The phase separation of the mixed chain length phosphatidylcholines revealed in these mixed bilayers may represent a three-dimensional phase separation of the lipid components where the phosphatidylcholines are both laterally separated within the plane of the bilayer and conformationally coupled across the bilayer. Such phase-separated domains could have profound effects on membrane structure and function if they were to occur in biological membranes.

The characterization of the lipid composition of biological membranes has revealed a rich diversity of lipid classes and subclasses (Ansell et al., 1973). These observations have stimulated interest in the thermodynamic properties of lipid mixtures and their relationship to membrane organization and function. The properties of binary mixtures of phospholipids that differ in their headgroup type or acyl chain composition have been studied by a variety of techniques. These include DSC[1] (Mabrey & Sturtevant, 1976; Silvius, 1986; van Dijck et al., 1977; Silvius & Gagné, 1984a,b), dilatometry (Wilkinson & Nagle, 1979; Schmidt & Knoll, 1986), ESR and NMR spectroscopy (Shimshick & McConnell, 1973; Wu & McConnell, 1975; Blume et al., 1982), freeze–fracture electron microscopy (Luna & McConnell, 1978), and Raman and IR spectroscopy (Mendelsohn & Maisano, 1978; Jaworsky & Mendelsohn, 1985). Theoretical descriptions of binary mixtures of phospholipids have also appeared (Jacobs et al., 1977; Priest, 1980; Sugar & Monticelli, 1985; Lee, 1977).

Numerous studies have examined the behavior of binary mixtures of different phospholipid species where the phospholipids have different polar headgroups but identical acyl chain compositions. These systems are characterized by complete miscibility of the phospholipid components in the liquid-crystalline phase and complete or limited miscibility of the phospholipid components in the bilayer gel phase. Examples include binary mixtures of PC and PE (Silvius, 1986), PC and PS and also PE and PS in the absence of calcium (Silvius & Gagné, 1984a,b), and PC and PG (Findlay & Barton, 1978). The mixing behavior of phospholipids in the gel phase of two-component bilayers is strongly influenced by differences in the acyl chain composition of the two phospholipid components. For binary mixtures of phosphatidylcholine, Curatolo et al. (1985) have observed that the PC components are completely or partially miscible in the gel phase when the absolute difference in the transition temperatures (ΔT_m) of the pure components is less than 33 °C. When the value of ΔT_m is greater than 33 °C, gel phase immiscibility is observed over a large compositional range. This general behavior appears to hold irrespective of whether the acyl chains are saturated, unsaturated, or of a mixed-acyl variety (Curatolo et al., 1985).

Of particular interest for the current study is the behavior of binary mixtures of phosphatidylcholines where one component is C(18)C(18)PC and the second component is C(16)C(16)PC, C(14)C(14)PC, or C(12)C(12)PC. It is observed that C(18)C(18)PC and C(16)C(16)PC, which differ in acyl chain length by two methylene units ($\Delta C = 2$), are completely miscible in both the L_β' and P_β' gel phases, even through the mixing is nonideal (Shimshick & McConnell, 1973; Matubayasi et al., 1986). The mixing behavior of C(18)C(18)PC and C(14)C(14)PC, where $\Delta C = 4$, has been

†This work was supported in part by Research Grant GM-33040 from the National Institute of General Medical Sciences, NIH, U.S. Public Health Service.

*Address correspondence to the author at the Department of Cellular Pathology, Armed Forces Institute of Pathology, Washington, DC 20306-6000.

[1] Abbreviations: PC, phosphatidylcholine; PE, phosphatidylethanolamine; PS, phosphatidylserine; PG, phosphatidylglycerol; C(x)C(y)PC, saturated diacylphosphatidylcholine with x carbons in the *sn*-1 chain and y carbons in the *sn*-2 chain; DSC, differential scanning calorimetry; Tris, tris(hydroxymethyl)aminomethane; C(24)SPM, (*N*-lignoceroylsphingosyl)phosphocholine; ESR, electron spin resonance; EDTA, ethylenediaminetetraacetic acid.

0006-2960/88/0427-4421$01.50/0

a point of considerable controversy. The DSC studies of Mabrey and Sturtevant (1976) and dilatometry studies of Wilkinson and Nagle (1979) have failed to reveal monotectic behavior in the gel phase, even though the mixing was observed to be strongly nonideal. However, other DSC studies (van Dijck et al., 1977; Matubayasi et al., 1986) as well as neutron scattering (Knoll et al., 1981) and dilatometry (Schmidt & Knoll, 1986) investigations have suggested that regions of gel phase immiscibility, possibly with peritectic phase behavior, exist in this system. For bilayers composed of C(18)C(18)PC and C(12)C(12)PC [C(18)C(18)PC–C(12)C(12)PC], where $\Delta C = 6$, there is strong evidence of immiscibility (lateral phase separation) in the gel phase over the compositional range of 0–80 mol % C(12)C(12)PC (Mabrey & Sturtevant, 1976). However, alternate distributions of the immiscible components, such as separation across the bilayer, might also be possible (Schimshick & McConnell, 1973). Over this compositional range, the bilayers appear to be segregated into phases of relatively pure C(12)C(12)PC and phases of C(18)C(18)PC saturated with C(12)C(12)PC. In all of the above systems, there is no evidence of immiscibility in the liquid-crystalline phase.

This laboratory has been engaged in the study of saturated mixed-chain phosphatidylcholines where the constituent acyl chains are asymmetric in length (Mason et al., 1981b; Huang et al., 1983; Hui et al., 1984). In the current investigation, the above studies have been extended by examining the mixing behavior of two-component bilayers composed of C(18)C(18)PC and either C(18)C(16)PC, C(18)C(14)PC, C(18)C(12)PC, or C(18)C(10)PC. It is found that mixed bilayers of C(18)C(18)PC–C(18)C(12)PC or C(18)C(18)PC–C(18)C(10)PC exhibit partial immiscibility of the components in the bilayer gel phase. Over a large compositional range, these bilayers are proposed to consist of segregated regions of interdigitated and noninterdigitated gel phases. In addition, the C(18)C(18)PC–C(18)C(10)PC two-component bilayers display a limited region of liquid–liquid immiscibility in the liquid-crystalline phase.

Materials and Methods

Synthesis and Purification of Phospholipids. Synthetic C(18)C(18)PC (lot C180-45) was purchased from Avanti Polar Lipids, Inc., Birmingham, AL. The mixed-acyl PCs C(18)C(16)PC, C(18)C(14)PC, C(18)C(12)PC, and C(18)C(10)PC were synthesized and purified by established procedures (Mason et al., 1981a). The mixed-acyl PCs were ≥98 mol % isomerically pure with regard to the positional specificity of the acyl chains on the glycerol backbone of the PCs. All of the phospholipids were precipitated twice from acetone/chloroform (95:5), dried under vacuum over $CaSO_2$, and finally stored as dry powders under nitrogen at −20 °C until used. The phospholipids were analyzed by thin-layer chromatography on 250-μM silica gel G plates by employing a solvent system of chloroform/methanol/28% ammonium hydroxide (65:35:5) and were then visualized with iodine. In all cases only a single spot, corresponding to authentic phospholipid, was observed at a loading of about 1 μmol of lipid.

Preparation of Samples for Calorimetry. The dry phospholipids were dissolved in chloroform at a concentration of about 10 mg/mL. The exact phospholipid concentrations were then determined by the method of inorganic phosphate (Gomori, 1942) subsequent to acid digestion of the samples. The phospholipid solutions were mixed volumetrically to produce the desired binary combinations of C(18)C(18)PC and one of the various mixed-acyl PCs. The phospholipid mixtures were dried under vacuum, redissolved in benzene, frozen, and lyophilized. This yielded fine, dry powders of the PC mixtures.

The PC mixtures were heated in a water bath at 60 °C for 30 min. This temperature is 5 °C above the T_m of C(18)C(18)PC, which is the highest melting component in all of the mixtures. A volume of 3 mL of buffer (50 mM KCl, 5 mM EDTA, and 10 mM Tris, pH 8.2) also heated to 60 °C was then added to each of the PC mixtures. The PC dispersions were thoroughly mixed and allowed to equilibrate at 60 °C for 12 h. Following determination of the PC concentration by phosphate analysis (as described above), the total phospholipid concentration in each of the preparations was adjusted to 15 mg/mL by dilution with buffer. The PC solutions were then cooled to 0 °C and incubated for 12 h. After the PC solutions were reheated to 60 °C and incubated for 12 h, the samples were cooled to 0 °C at a rate of 5 °C/h. The preparations were then incubated at 0 °C for 30 days prior to analysis by DSC.

Differential Scanning Calorimetry. All DSC runs were performed on a Microcal MC-2 differential scanning calorimeter (Microcal, Inc., Amherst, MA). The calorimeter is equipped for microcomputer control of data acquisition and analysis. The sample and 3 mL of buffer were placed in an ice bath and degassed under vacuum for 30 min. Approximately 1 mL each of the sample and buffer was then loaded into the sample and reference cells, respectively, of the calorimeter. The calorimeter had been preequilibrated at 0 °C prior to loading. The sample and buffer were allowed to come to thermal equilibrium, typically 1 h, prior to the initiation of the scan. All scans were performed in the ascending temperature mode at a scan rate of 10 °C/h. Two (or three) DSC runs were performed for each unique composition of the four binary mixtures. These runs were performed with aliquots of separate dispersions prepared from the same two lots of phospholipids.

The calorimetric data were analyzed to yield phospholipid excess heat capacities as a function of temperature and transition enthalpy changes by employing the software supplied by Microcal. The phospholipid concentrations of the preparations were determined by phosphate analyses of aliquots of the degassed samples employed to load the calorimeter. The phospholipid concentrations employed (~15 mg/mL) were much higher than necessary on the basis of the sensitivity of the instrument. These high sample loadings were used in order to ensure flat base lines for accurate determination of the onset and completion temperatures of the thermal transitions. All phospholipid preparations were analyzed by thin-layer chromatography (as described above) following the calorimetric scans. In all cases, no degradation of the phospholipids was detected.

Results

C(18)C(18)PC–C(18)C(16)PC. Excess heat capacity profiles of multilamellar dispersions of C(18)C(18)PC, C(18)C(16)PC, and a 1:1 mixture of C(18)C(18)PC–C(18)C(16)PC are shown in Figure 1. Aqueous preparations of C(18)C(18)PC (T_m = 54.4 °C, ΔH = 10.3 kcal/mol) and C(18)C(16)PC (T_m = 44.1 °C, ΔH = 7.6 kcal/mol) display sharp gel to liquid-crystalline phase transitions. The thermodynamic parameters observed for these single-component bilayers agree well with those obtained in previous studies (Mason et al., 1981b; Chen & Sturtevant, 1981). Dispersions consisting of an equimolar mixture of C(18)C(18)PC and C(18)C(16)PC display a broadened ($\Delta T_{1/2}$ = 1.5 °C) main transition peak (T_m = 49.8 °C). This excess heat capacity profile is slightly asymmetric; it is broader on the low-temperature side of the transition for temperatures less than T_m.

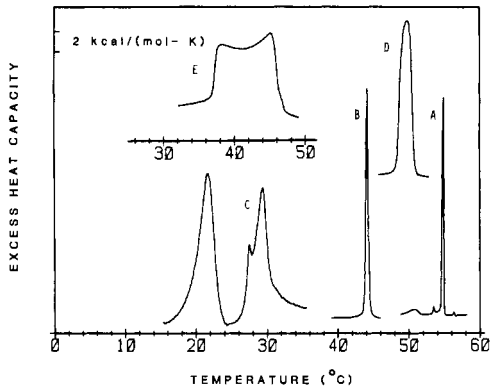

FIGURE 1: DSC profiles of the single-component multilamellar bilayers C(18)C(18)PC (A), C(18)C(16)PC (B), and C(18)C(14)PC (C) and also of multilamellar bilayers of 1:1 (mol/mol) binary mixtures of C(18)C(18)PC with C(18)C(16)PC (D) or C(18)C(14)PC (E). Total phospholipid concentrations were 10–15 mg/mL in excess buffer. The samples were cooled at 5 °C/h from a temperature above the thermal completion temperature of the respective phase transitions to 0 °C and then incubated at this temperature for 30 days prior to analysis by DSC. Samples were scanned at 10 °C/h in an ascending temperature mode.

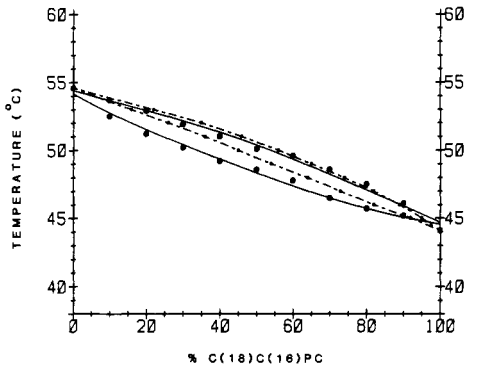

FIGURE 2: Phase diagram for the C(18)C(18)PC–C(18)C(16)PC binary system. The solidus line (lower solid line) is derived from the thermal onset temperatures (T_0) of the main transition, and the fluidus line (upper solid line) is derived from the thermal completion temperatures (T_c) of the main transition. The T_0 and T_c values have been corrected to account for the finite transition widths of the pure components. The dotted lines represent the ideal phase diagram for this binary system calculated as described in the text.

The transition curves for a series of C(18)C(18)PC–C(18)C(16)PC multilamellar dispersions containing various mole percent concentrations of C(18)C(16)PC (data not shown) all display fairly sharp, slightly asymmetric main transition peaks. The onset (T_0) and completion (T_c) temperatures of these main transitions are plotted as a function of C(18)C(16)PC content in Figure 2. The T_0 and T_c values for each composition represent the average values from two DSC runs. The standard deviations for the transition temperatures are <0.5 °C. The transition widths have been corrected to account for the finite transition widths of the pure components according to the procedure of Mabrey and Sturtevant (1976). The solid lines in Figure 2 are second-degree polynomial fits to the experimental data. Also shown in Figure 2 is the ideal phase diagram (dotted lines) for this binary system derived from the equations given by Mabrey and Sturtevant (1976). The thermal onset temperatures define the solidus line below which the bilayer consists of a single gel phase. Likewise, the thermal completion temperatures define the fluidus line above which the bilayer consists of a single fluid phase. The area between these lines defines the coexistence region where the bilayer consists of solid and fluid domains laterally separated in the plane of the bilayer (Shimshick & McConnell, 1973). Both the solidus and fluidus lines are smooth curves that have no discontinuities. Thus, C(18)C(18)PC and C(18)C(16)PC exhibit complete miscibility in both the gel and liquid-crystalline phases over the entire compositional range. In addition, the mixture displays only slight negative deviation from ideal behavior. In accordance with the above observations, the main peak transition temperatures are found to vary linearly with composition [$T_m = X_1T_1 + (1 - X_1)T_2$, where T_1 and T_2 are the main transition temperatures of C(18)C(18)PC and C(18)C(16)PC, respectively, and X_1 is the mole fraction of C(18)C(16)PC in the mixture]. This same linear behavior is observed for the main transition enthalpies (enthalpy changes) of the binary mixtures. The latter observation implies that the excess enthalpy of mixing of the two components is similar in the gel and liquid-crystalline phases.

Dispersions of C(18)C(18)PC display a thermal pretransition from the $L_{\beta'}$ to $P_{\beta'}$ phase at T_p = 51.7 °C (ΔH = 2.1 kcal/mol). If aqueous preparations of C(18)C(16)PC are cooled from a temperature above the main transition and then immediately scanned from the low temperature, a $L_{\beta'}$ to $P_{\beta'}$ pretransition is observed at T_p = 30.1 °C (ΔH = 0.7 kcal/mol). However, the $L_{\beta'}$ gel phase is metastable and converts to a highly ordered crystalline L_c subphase following prolonged incubation. This leads to the observation of an L_c to $P_{\beta'}$ subtransition at T_s = 33.2 °C (ΔH = 5.1 kcal/mol) (Stümpel et al., 1983; Serrallach et al., 1984). Incubation of C(18)C(18)PC–C(18)C(16)PC mixtures at 0 °C for 3 weeks leads to the appearance of poorly resolved, low-temperature transitions, which were not analyzed. However, if the mixtures are scanned immediately after being cooled from a temperature above the main transitions, a series of pretransitions are observed. Plots of the corrected onset and completion temperatures (data not shown) indicate nearly ideal mixing of the lipids in the $L_{\beta'}$ and $P_{\beta'}$ phases. Thus, the main transitions of this binary system represent the transformation of the $P_{\beta'}$ gel phase to the L_α phase over the entire range of compositions. It should also be noted that the main transitions of the C(18)C(18)PC–C(18)C(16)PC dispersions did not display a dependence upon thermal history. Scans conducted immediately following cooling from 60 °C were identical with those conducted following incubation at 0 °C for 3 weeks.

C(18)C(18)PC–C(18)C(14)PC. Excess heat capacity profiles of aqueous dispersions of C(18)C(14)PC and an equimolar mixture of C(18)C(18)PC–C(18)C(14)PC are also shown in Figure 1. Multilamellar bilayers of C(18)C(14)PC exhibit a main gel to liquid-crystalline phase transition at T_m = 29.8 °C (ΔH = 5.6 kcal/mol). The excess heat capacity profile of this main transition is highly asymmetric in shape, which arises from the heterogeneous distribution of liposomal sizes in these preparations (Mason et al., 1983). Following prolonged incubation at 0 °C, C(18)C(14)PC dispersions display a subtransition at T_s = 23.4 °C (ΔH = 6.4 kcal/mol) (Huang & Mason, 1986; Stümple et al., 1983). This subtransition is a transition from a crystalline L_c subphase to a $P_{\beta'}$ gel phase. If dispersions of C(18)C(14)PC are scanned immediately subsequent to cooling from a temperature above the main transition, an $L_{\beta'}$ to $P_{\beta'}$ pretransition is observed at T_p = 19.1 °C (ΔH = 1.3 kcal/mol) (Mason et al., 1981b; Chen & Sturtevant, 1981).

Dispersions of an equimolar mixture of C(18)C(18)PC–C(18)C(14)PC exhibit a broad, asymmetric transition that spans the range from 34.6 to 47.8 °C ($\Delta T_{1/2}$ = 7.2 °C, ΔH = 9.6 kcal/mol). The asymmetry of the transition profile is reminiscent of that observed for mixtures of C(18)C(18)PC and C(14)C(14)PC (Mabrey & Sturtevant, 1976). The corrected

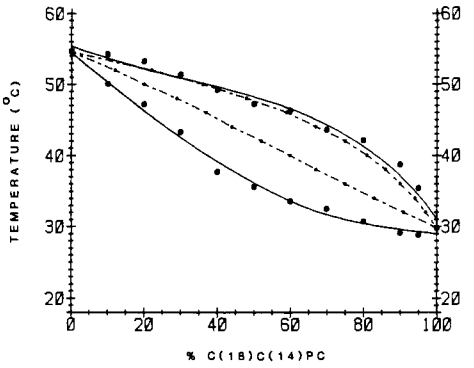

FIGURE 3: Phase diagram for the C(18)C(18)PC–C(18)C(14)PC binary system. Other conditions were as described in Figure 2.

onset and completion temperatures for a series of C(18)C(18)PC–C(18)C(14)PC mixtures are plotted in Figure 3 along with the ideal phase diagram for this system. The T_0 and T_c values for each composition represent the average values from two DSC runs. The standard deviations for the transition temperatures are <0.8 °C. The fluidus line is obtained as a second-degree polynomial fit to the data, and the solidus line is a third-degree polynomial fit to the data. The fluidus line is virtually superimposable upon the ideal fluidus line. The solidus line, in contrast, displays strong negative deviation from ideal behavior. Despite the irregular shape of the solidus curve, it is continuous and has no sharp points of inflection. In addition, no horizontal portion, or region of isothermal melting, is observed. These characteristics lead to the conclusion that C(18)C(18)PC and C(18)C(14)PC are miscible in all proportions in the gel and liquid-crystalline phases. However, the intermixing of the lipids is highly nonideal in the low-temperature phase. The nonideality of this system, as observed in the phase diagram, is also seen in the transition enthalpies. In the range of 5–30 mol % C(18)C(14)PC, the transition enthalpies are nearly ideal. From 30 to 95 mol % C(18)C(14)PC, the observed transition enthalpies are, on the average, 1.19 times the ideal values.

Over the range of 5–30 mol % C(18)C(14)PC, the excess heat capacity profiles of the C(18)C(18)PC–C(18)C(14)PC mixtures display broad, poorly resolved pretransitions ranging in transition temperature from 30 to 44 °C. Above 30 mol % C(18)C(14)PC, no low-temperature transitions are observed after 3 weeks of incubation at 0 °C. These observations are intriguing in view of the ability of C(18)C(14)PC bilayers to form an L_c crystalline subphase.

C(18)C(18)PC–C(18)C(12)PC. A series of thermograms obtained with C(18)C(18)PC–C(18)C(12)PC dispersions of various C(18)C(12)PC content are shown in Figure 4. Multilamellar bilayers of pure C(18)C(12)PC exhibit a main gel to liquid-crystalline phase transition at T_m = 17.9 °C (ΔH = 10.4 kcal/mol). The excess heat capacity profile of this PC is asymmetric with a shoulder on the high-temperature side of the profile. This asymmetry remains even after prolonged incubation of the sample at low temperatures (Huang & Mason, 1986). Preparations containing 10–20 mol % C(18)C(12)PC exhibit a broad, low-temperature endotherm that spans the range from 18 to 33 °C ($\Delta T_{1/2}$ = 6.6 °C). A high-temperature endotherm is also apparent, and it displays a shape that suggests that it arises from a phase rich in C(18)C(18)PC nonideally mixed with a smaller amount of the mixed-chain component. Over the compositional range of 20–60 mol % C(18)C(12)PC, the low-temperature endotherm sharpens considerably ($\Delta T_{1/2} \simeq$ 2.2 °C) while the onset temperature remains fixed at about 17.7 °C. In contrast, the high-temperature endotherm continues to broaden while the completion temperature drops from 48 to 43 °C. From 70 to 90 mol % C(18)C(12)PC, the low-temperature transition first broadens and then narrows again. At the same time, the onset temperature decreases from 17.7 to 15.3 °C. The high-temperature portion of the transition profile continues to decrease in magnitude and broaden until it finally merges with the low-temperature peak. The completion temperature decreases from 43 to 35 °C. Clearly, this system displays highly nonideal behavior. The nonideality of the system is also reflected in the transition enthalpies. Over the range of 5–30 mol % C(18)C(12)PC, the transition enthalpies are, on the average, about 1.15 times the ideal values; whereas from 35 to 95 mol % C(18)C(12)PC, they are about 0.92 times the ideal values.

The phase diagram for the C(18)C(18)PC–C(18)C(12)PC system is shown in Figure 5. The T_0 and T_c values for each

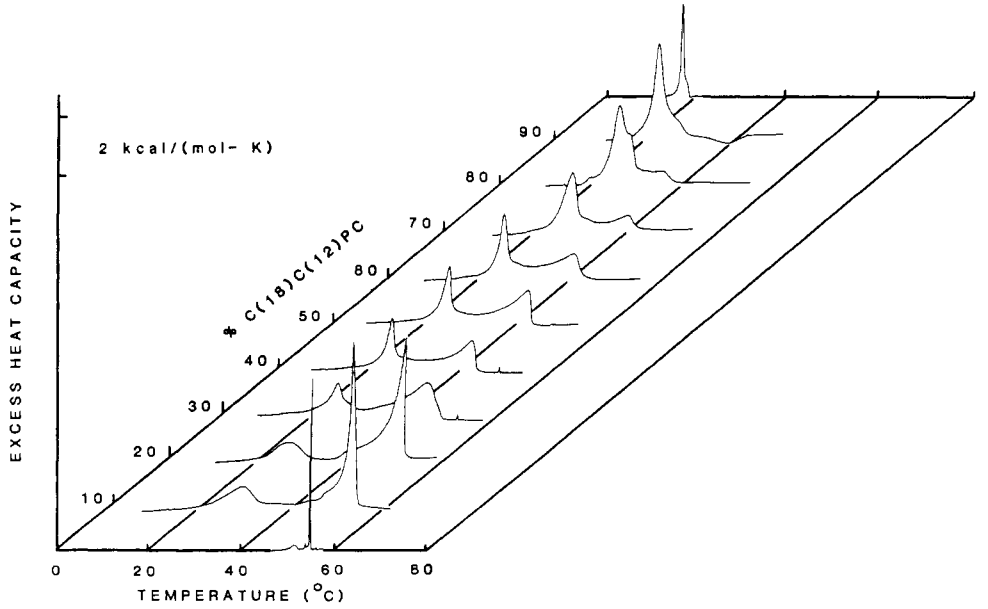

FIGURE 4: A series of thermograms obtained with C(18)C(18)PC–C(18)C(12)PC multilamellar bilayers of various C(18)C(12)PC contents. The excess heat capacity scale has been reduced by a factor of 4 for the DSC traces of the single-component bilayers. Other conditions were as described in Figure 1.

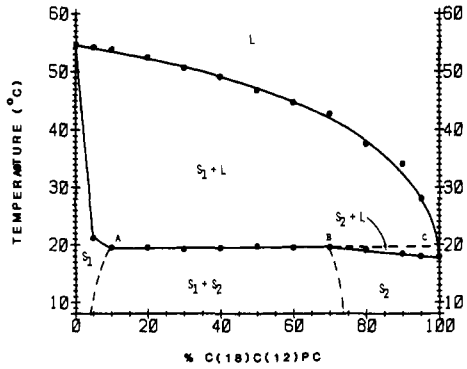

FIGURE 5: Phase diagram for the C(18)C(18)PC–C(18)C(12)PC binary system. The solid lines are the experimentally determined phase boundaries. The dashed lines are inferred phase boundaries. The various phase designations are discussed in the text. Other conditions were as described in Figure 2.

composition represent the average values from two to three DSC runs. The T_0 values are highly reproducible with standard deviations of <0.7 °C. Due to the breadth of the transitions, the T_c values are more variable and differ by not more than 1.5 °C for a given composition. However, the standard deviations are always <1.2 °C. The fluidus line is obtained as a third-degree polynomial fit to the experimentally observed values. The observed fluidus line exhibits only slight negative deviation from the ideal fluidus line (not shown). Over the range of 10–65 mol % C(18)C(12)PC, a region of isothermal melting is observed. This is indicative of a region of three-phase coexistence. However, the fact that the isothermal melting temperature is higher than the transition temperature of pure C(18)C(12)PC suggests that this region represents the melting of a solid solution. This is characteristic of a system where the components exhibit partial miscibility. From 70 to 95 mol % C(18)C(12)PC, the melting temperature decreases in a linear fashion and extrapolates to the transition temperature of pure C(18)C(12)PC. The details of the phase diagram are addressed under Discussion.

The thermograms of the C(18)C(18)PC–C(18)C(12)PC binary mixtures display a strong dependence upon the thermal history (data not shown). If samples are scanned immediately after being cooled from 65 °C, the low-temperature endotherm is not seen, and no region of isothermal melting is observed. The thermograms are similar to those seen for the nonideally mixed C(18)C(18)PC–C(18)C(14)PC system. Only after 1 h of incubation at 0 °C does the low-temperature endotherm begin to emerge. However, isothermal melting is only observed in samples that have been incubated at 0 °C for several hours. The series of thermograms shown in Figure 4 do not change following additional incubation at 0 °C.

C(18)C(18)PC–C(18)C(10)PC. A series of thermograms obtained with C(18)C(18)PC–C(18)C(10)PC dispersions of various C(18)C(10)PC content are shown in Figure 6. Multilamellar dispersions of pure C(18)C(10)PC display a main gel to liquid-crystalline phase transition at T_m = 19.1 °C (ΔH = 9.9 kcal/mol). This transition is observed to be quite broad for dispersions of a pure PC ($\Delta T_{1/2}$ = 0.98 °C) when samples are scanned immediately after being cooled from 25 °C (Mason et al., 1981b). The transition narrows considerably ($\Delta T_{1/2}$ = 0.29 °C) when samples are incubated for prolonged periods at 0 °C prior to DSC analysis (Huang & Mason, 1986). The thermograms for binary preparations containing 5–40 mol % C(18)C(10)PC strongly resemble the corresponding thermograms observed for the C(18)C(18)PC–C(18)C(12)PC system with the exception of the presence of the sharp endotherm at 45.5 °C, which will be discussed below. A broad ($\Delta T_{1/2}$ = 4.6 °C) low-temperature endotherm is seen, which spans the range from 19 to 35 °C. The onset temperature for this endotherm remains fixed at about 19.5 °C. A high-temperature endotherm is also apparent and is suggestive of a phase rich in C(18)C(18)PC nonideally mixed with a smaller amount of the mixed-chain component. This endotherm broadens while the completion temperature decreases from 54 to 51 °C. At 50 mol % C(18)C(10)PC, the character of the transition profiles change dramatically. A sharp low-temperature endotherm slowly emerges whose onset temperature, about 17.5 °C, is identical with that observed for pure C(18)C(10)PC. From 50 to 70 mol % C(18)C(10)PC, the remainder of the transition profile consists of a broad high-temperature component and an additional broad feature with an apparent peak temperature of 26–29 °C. Finally, from 80 to 95 mol % C(18)C(10)PC, the broad high-temperature features become reduced in magnitude and merge with the sharp low-temperature endotherm. The completion temper-

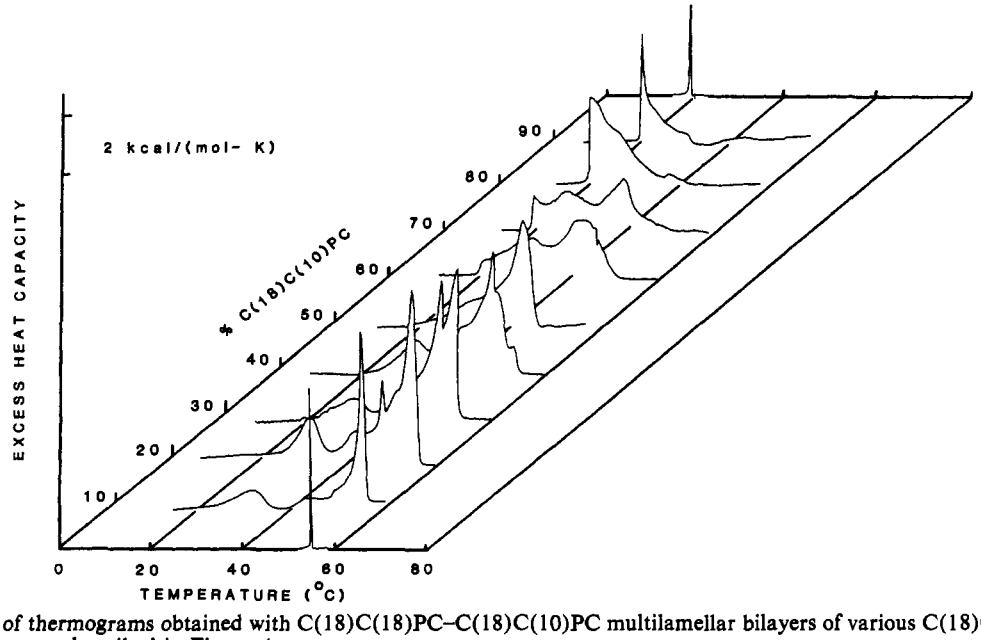

FIGURE 6: A series of thermograms obtained with C(18)C(18)PC–C(18)C(10)PC multilamellar bilayers of various C(18)C(10)PC contents. Other conditions were as described in Figure 4.

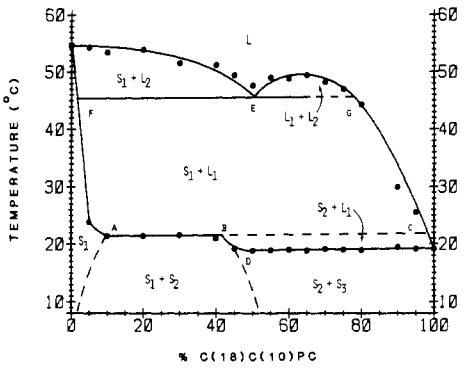

FIGURE 7: Phase diagram for the C(18)C(18)PC–C(18)C(10)PC binary system. Other conditions were as described in Figures 2 and 5.

ature drops sharply from 46 to 26 °C over this compositional range.

The phase diagram for the C(18)C(18)PC–C(18)C(10)PC system is shown in Figure 7. The T_0 and T_c values for each composition represent the average values from two to three DSC runs. The T_0 values are highly reproducible with standard deviations of <0.6 °C. Due to the breadth of the transitions, the T_c values are more variable and differ by not more than 1.6 °C for a given composition. However, the standard deviations are always <1.3 °C. Over the compositional range of 10 to 40 mol % C(18)C(10)PC, a region of isothermal melting is observed at 21.2 °C. This is indicative of a region of three-phase coexistence. As is the case for the C(18)C(18)PC–C(18)C(12)PC system, the fact that the isothermal melting temperature is higher than the transition temperature of pure C(18)C(10)PC suggests that this region represents the melting of a solid solution. Again, this is characteristic of a system exhibiting partial miscibility of the components. From 50 to 95 mol % C(18)C(10)PC, a second region of isothermal melting is observed at 19 °C. In this case, the isothermal melting temperature corresponds to the transition temperature of pure C(18)C(10)PC. This indicates that one of the three phases present at equilibrium at this temperature is a solid phase of pure C(18)C(10)PC.

In many of the thermograms, a sharp endothermic peak is observed at 45.5 °C. This endotherm is first seen in the 10 mol % C(18)C(10)PC sample and increases in magnitude up to the 40 mol % C(18)C(10)PC sample. The endotherm cannot be seen in the 50 mol % sample but may be obscured by the high-temperature endothermic component of the transition profile. The 45.5 °C peak is again seen in the 60 and 70 mol % samples, but it is reduced in magnitude. This sharp endothermic feature is assigned to a region of three-phase coexistence in the phase diagram at 45.5 °C. This is interpreted to indicate the existence of a region of liquid–liquid immiscibility in the liquid-crystalline phase of this binary system.

Over the compositional range of about 50–75 mol % C(18)C(10)PC, the solid phase melts to produce two immiscible liquid phases, one (L_1) enriched in C(18)C(10)PC and a second (L_2) enriched in C(18)C(18)PC. At about 60 mol % C(18)C(10)PC, these two immiscible liquids exist over a maximal temperature range of about 4 °C and terminate at a critical solution temperature of 49 °C. The compositional dependence of the transition enthalpies was observed to reflect the nonideality of this system. In general, the trends are similar to those obtained for the C(18)C(18)PC–C(18)C(12)PC system. Additional features of the phase diagram and the dependence of this binary system on the thermal history of the samples will be addressed under Discussion.

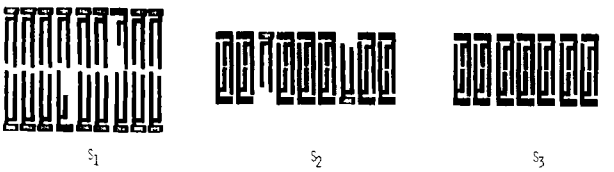

FIGURE 8: Molecular diagrams of the proposed conformational chain packings existing within the various gel phases exhibited by the C(18)C(18)PC–C(18)C(12)PC and C(18)C(18)PC–C(18)C(10)PC mixed bilayers: S_1, a solid solution characterized by noninterdigitation of the acyl chains of the phosphatidylcholines; S_2, a solid solution where the mixed-chain component adopts a mixed interdigitated packing and the symmetric chain component is fully interdigitated; S_3, a phase consisting of pure C(18)C(10)PC in a mixed interdigitated packing conformation.

Discussion

This laboratory has been engaged in the study of the effects of an asymmetry in the length of the two constituent acyl chains on the bilayer properties of saturated mixed-chain phospholipids (Mason et al., 1981b; Huang et al., 1983; Hui et al., 1984; Huang & Mason, 1986). One of our motivations for studying chain length asymmetries in saturated mixed-chain phosphatidylcholines was the observation that binary mixtures of saturated symmetric chain phosphatidylcholines differing in chain length by six methylene units are monotectic and show lateral phase separation in the gel state (Mabrey & Sturtevant, 1976). The saturated mixed-chain phosphatidylcholines represent an interesting variation on the above studies, since the acyl chains are forced to mix because they are attached to the same glycerol backbone. The bilayer's response to this dilemma is to compensate for the phosphatidylcholine chain length asymmetry by adopting a gel phase packing arrangement where the acyl chains interdigitate across the bilayer centers. Thus, as the chain length asymmetry in the saturated mixed-chain phosphatidylcholines is increased, a transformation from a noninterdigitated to a partially interdigitated, to a mixed interdigitated, and then finally to a fully interdigitated gel phase lamellar packing is observed (Huang & Mason, 1986). Of relevance to the current study are the studies on the saturated phosphatidylcholine series C(18)C(18)PC, C(18)C(16)PC, C(18)C(14)PC, C(18)C(12)PC, and C(18)C(10)PC. Bilayers composed of C(18)C(18)PC or C(18)C(16)PC do not show significant interdigitation of the phospholipid's hydrocarbon chains across the bilayer center in the gel phase (Stümpel et al., 1983; Huang & Mason, 1986). Raman spectroscopic (Huang et al., 1983) and X-ray diffraction (Hui et al., 1984) studies indicate that the acyl chains of the C(18)C(14)PC molecules do not interdigitate in the gel phase of this bilayer system. Instead, the C(18)C(14)PC gel phase bilayer is characterized by a region of highly disordered acyl chain terminals sandwiched by relatively ordered chain segments (Hui et al., 1984). However, prolonged incubation of aqueous assemblies of C(18)C(14)PC at low temperatures leads to the formation of an L_c crystalline subphase. In the L_c subphase, the acyl chains of the C(18)C(14)PC molecules are partially interdigitated so that the short chain of one lipid packs end to end with the long chain of another lipid in the opposing leaflet of the bilayer (Stümpel et al., 1983). X-ray diffraction studies by Hui et al. (1984) and McIntosh et al. (1984) have demonstrated that the bilayer gel phases of C(18)C(12)PC and C(18)C(10)PC adopt a packing conformation where the short chains of the phosphatidylcholines from opposing leaflets pack end to end and the long chains span the entire width of the hydrocarbon core of the bilayer. This has been termed a mixed interdigitated bilayer (see S_3 of Figure 8).

C(18)C(18)PC–C(18)C(16)PC. Bilayers of C(18)C(18)PC and C(18)C(16)PC show complete miscibility of the components over the entire range of composition. The results obtained here suggest that the bilayers consist of a single P_{β}' gel phase at temperatures just below the main gel to liquid-crystalline transition temperatures. In addition, this system displays only a slight negative deviation from ideal behavior. This deviation is smaller than that displayed by binary mixtures of symmetric chain phosphatidylcholines that differ in chain length by two methylene units, such as C(18)C(18)PC–C(16)C(16)PC (Matubayasi et al., 1986) and C(16)C(16)PC–C(14)C(14)PC (Mabrey & Sturtevant, 1976). This is not unexpected since the effective difference in chain length in the C(18)C(18)PC–C(18)C(16)PC system is less than that present in the above symmetric chain phosphatidylcholine binary mixtures.

C(18)C(18)PC–C(18)C(14)PC. Bilayers of C(18)C(18)PC and C(18)C(14)PC also show miscibility of the components over the entire range of composition. However, the mixing in the bilayer gel phase is highly nonideal. It is important to note that the solidus line does not display any points of inflection or any regions of isothermal melting. Thus, although the mixing of the components is clearly nonideal, no lateral phase separation of the components occurs in the bilayer gel phase of this system. The nonideality displayed by this system is not as great as that observed in the C(18)C(18)PC–C(14)C(14)PC symmetric phosphatidylcholine binary mixture. Again, this suggests that the gel phase packing properties of the binary mixture are not strictly determined by the length of the shorter chain of the mixed chain length phosphatidylcholine component. The C(18)C(18)PC–C(18)C(14)PC system displays a series of pretransitions from 5 to 30 mol % C(18)C(14)PC, but no other low-temperature transitions are observed outside of this compositional range. This suggests that the bilayer packs in a noninterdigitated conformation over the entire range of compositions. The C(18)C(14)PC component is prevented from forming a crystalline subphase because it is unable to interdigitate across the bilayer center. A lateral separation of the C(18)C(14)PC components would probably be a prerequisite to the formation of an interdigitated packing arrangement as is shown below.

C(18)C(18)PC–C(18)C(12)PC. The behavior of binary mixtures of C(18)C(18)PC and C(18)C(12)PC can be explained by postulating that the two components exhibit partial miscibility in the bilayer gel phase. Consider the effect of an increase in C(18)C(12)PC content at a constant temperature of 12 °C. As small amounts of C(18)C(12)PC are added to the mixture a single phase, S_1, is formed. The packing conformation proposed for phase S_1 is shown in Figure 8. This phase is enriched in C(18)C(18)PC, and the acyl chains pack without interdigitating across the bilayer center. The C(18)C(12)PC present in the phase is also not interdigitated. This probably requires the displaced ends of the stearoyl chains to conformationally disorder so as to fill the void region beneath the short dodecanoyl chains and maximize van der Waals contacts (Mason et al., 1981b). At some point, the solubility limit of C(18)C(12)PC in phase S_1 is reached. This has been estimated to be 5 mol % C(18)C(12)PC in the phase diagram of Figure 5. A different technique, such as FT-IR spectroscopy, will be required to establish the exact position of the solid phase boundaries. At this point, the further addition of C(18)C(12)PC leads to the formation of a new phase, S_2. As shown in Figure 8, phase S_2 is enriched in C(18)C(12)PC, which packs in a mixed interdigitated conformation. The C(18)C(18)PC present in this phase is probably fully interdigitated. A fully interdigitated conformation has been observed for a number of symmetric chain phospholipid bilayers under a variety of conditions (Simon & McIntosh, 1984; Boggs et al., 1981; Small, 1984). The composition of phase S_2 is estimated to be 75 mol % C(18)C(12)PC in the phase diagram of Figure 5. As the amount of C(18)C(12)PC in the mixture is increased within this two-phase region, the compositions of phases S_1 and S_2 remain fixed. However, the amount of phase S_2 increases at the expense of phase S_1 as dictated by the lever rule. At 80 mol % C(18)C(12)PC (arbitrary), phase S_1 is completely consumed, and a single-phase region consisting of phase S_2 remains.

Consider now the effect of an increase in temperature at an isoplethic composition of 40 mol % C(18)C(12)PC. At 10 °C the bilayer gel phase consists of two phases, $S_1 + S_2$. When the temperature is increased to about 19.5 °C, the first melt is observed. Three phases are now present: S_1 with composition A (Figure 5); S_2 with composition B; and liquid-crystalline phase, L, with composition C. With three phases present, the system is invariant (Gibbs phase rule) and melts isothermally until one of the phases is consumed. In this case, the liquid-crystalline phase is more enriched in C(18)C(12)PC than either phase S_1 or phase S_2. Thus, phase S_2 is preferentially consumed leaving phases S_1 + L. The bilayer now enters a two-phase coexistence region. As the temperature is increased further, solid phase S_1 continues to melt, and liquid phase L becomes enriched in C(18)C(18)PC. Finally, at about 49 °C the last remnant of phase S_1 melts giving rise to a single liquid-crystalline phase. At 80 mol % C(18)C(12)PC, solid phase S_2 starts to melt at about 18.5 °C giving rise to a two-phase coexistence region consisting of phases S_2 + L. When the temperature reaches about 19.5 °C, three phases again coexist, $S_1 + S_2$ + L, and the system melts isothermally until phase S_2 is consumed.

C(18)C(18)PC–C(18)C(10)PC. The behavior of binary mixtures of C(18)C(18)PC and C(18)C(10)PC can be explained by postulating partial immiscibility of the components in both the gel and liquid-crystalline bilayer phases. Consider the effect of an increase in C(18)C(10)PC content at an isothermal temperature of 12 °C. From 0 to 50 mol % C(18)C(10)PC, the two components exhibit partial immiscibility in the bilayer gel phase. This gives rise to a two-phase region consisting of phases S_1 and S_2 between 5 and 50 mol % C(18)C(10)PC. Again, the assignments of the gel phase boundaries in the phase diagram of Figure 7 are estimates. This behavior is analogous to that observed for the C(18)C(18)PC–C(18)C(12)PC mixtures discussed above. At the solubility limit of C(18)C(18)PC in the S_2 phase [designated as about 50 mol % C(18)C(10)PC in Figure 7], the bilayer gel phase consists entirely of phase S_2. The further addition of C(18)C(10)PC results in the formation of a phase of pure C(18)C(10)PC, which is designated as S_3. The mixed interdigitated chain packing in phase S_3 is shown in Figure 8. This gives rise to a two-phase region consisting of phases $S_2 + S_3$ between 50 and 100 mol % C(18)C(10)PC. Now consider the effect of an increase in temperature at an isoplethic composition of 65 mol % C(18)C(10)PC. At 10 °C the bilayer consists of two phases, $S_2 + S_3$. When the temperature is increased to 19 °C, the first melt is observed. Three phases are now present: S_2 with composition D (Figure 7); S_3; and L_1, which, initially, is a liquid-crystalline phase consisting of pure C(18)C(10)PC. The system is invariant and melts isothermally until S_3 is completely consumed. The bilayer now enters a two-phase coexistence region consisting of $S_2 + L_1$. When the temperature is increased to about 22 °C, the bilayer

again consists of three phases: S_1 with composition A; S_2 with composition B; and L_1 with composition C. The system is invariant and melts isothermally until S_2 is completely consumed. Indeed, the broad endothermic feature centered near 24 °C in the transition profiles for the 50–70 mol % C(18)-C(10)PC samples may reflect, in part, this isothermal melting. The bilayer now enters a two-phase coexistence region consisting of $S_1 + L_1$. As the temperature is increased further, S_1 continues to melt and L_1 becomes progressively enriched in C(18)C(18)PC.

At 45.4 °C the solubility limit of C(18)C(18)PC in L_1 is reached, and a new liquid-crystalline phase, L_2, is formed, which is enriched in C(18)C(18)PC. The bilayer now consists of three phases: S_1 with composition F; L_2 with composition E; and L_1 with composition G. The system is again invariant and melts isothermally until one phase is completely consumed. As S_1 melts, the amount of C(18)C(10)PC liberated is not sufficient to form phase L_2. Thus, phase L_1 is consumed to supply the additional C(18)C(10)PC. However, at 65 mol % C(18)C(10)PC, the size of phase L_1 is larger than that of phase S_1. Thus, S_1 melts before L_1 is consumed. The bilayer now enters a region of two-phase coexistence consisting of two immiscible liquid-crystalline phases L_1 and L_2. Finally, at about 50 °C, a critical solution temperature is reached, and the bilayer enters a region consisting of a single liquid-crystalline phase. If the overall bilayer composition were 20 mol % C(18)C(10)PC, the system would contain more of phase S_1 than phase L_1 at 45.4 °C. In this case, L_1 would be consumed to form phase L_2 before all of phase S_1 melts. Thus, a two-phase region consisting of $S_1 + L_2$ would result.

Point E in the phase diagram of Figure 7 represents a eutectic point. Here, the system melts to form a liquid-crystalline phase whose composition is the same as that of the overall system. On the basis of the results from repeated DSC scans in this region, the eutectic point occurs at 46.2 ± 0.6 °C (mean ± 1 SD) and at a composition of 53 ± 3.2 mol % C(18)C-(10)PC (mean ± 1 SD). Also, the enthalpy of the 45.4 °C endotherm should be maximal at this composition. Indeed, from 10 to 40 mol % C(18)C(10)PC, this sharp endotherm clearly increases in enthalpy. The endotherm is obscured in the 50 mol % sample but clearly decreases in enthalpy from 60 to 70 mol % C(18)C(10)PC. From these observations it can be inferred that the endotherm goes through a maximum between 40 and 60 mol % C(18)C(10)PC.

The C(18)C(18)PC–C(18)C(10)PC system displays an interesting dependence upon thermal history. Samples of C(18)C(18)PC–C(18)C(10)PC were heated to 60 °C, cooled to 0 °C at 5 °C/h, and then incubated at this temperature for 1 h prior to analysis by DSC. The endothermic transition profiles for 20 and 60 mol % C(18)C(10)PC samples are shown in curves A and B of Figure 9, respectively. The 20 mol % C(18)C(10)PC sample fails to display the isothermal transition at 22 °C corresponding to the melting of phase S_2. This transition is only observed in samples that have been incubated at low temperatures for prolonged periods. Thus, the formation of the S_2 phase most likely proceeds by a nucleation and growth process. As can be seen in Figure 8, the bilayer thickness of phase S_2 is substantially less than that of phase S_1. There is a precedent for the coexistence of bilayer gel phases of dissimilar thicknesses. The behavior of binary mixtures of symmetric chain phospholipids of dissimilar chain lengths has been studied by Jacobs et al. (1977). This theoretical study concluded that such phospholipids pack with a relatively flat interface between the two bilayer leaflets. As a result, the phospholipids with the longer chains must penetrate further into the aqueous phase. The phospholipid molecules at the boundary between phases S_1 and S_2 must be characterized by a large hydrocarbon-packing free energy. Thus, only nuclei of phase S_2 that are of a critical size proceed to grow into large domains. This process requires prolonged incubation of the binary system. In contrast, the 60 mol % C(18)C(10)PC mixture of Figure 9B displays a much sharper endotherm at 19 °C, which corresponds to the melting of phase S_3, than is seen in samples that have been incubated for prolonged periods. As can be seen in Figure 8, phases S_2 and S_3 have similar bilayer thicknesses. The transition profile of Figure 9B suggests that slow cooling of the sample results in the formation of large domains of phase S_3, which, in turn, give rise to a sharp, cooperative transition. However, prolonged incubation of the sample at 0 °C results in considerable broadening of this transition, which suggests of a loss of cooperativity. This suggests that considerable intermixing of phases S_2 and S_3 occurs in the bilayer gel phase by diffusion within the plane of the bilayer. The hydrocarbon-packing free energy of the C(18)C(10)PC molecules in phase S_3 may be only marginally smaller than that for C(18)C(10)PC molecules in phase S_2.

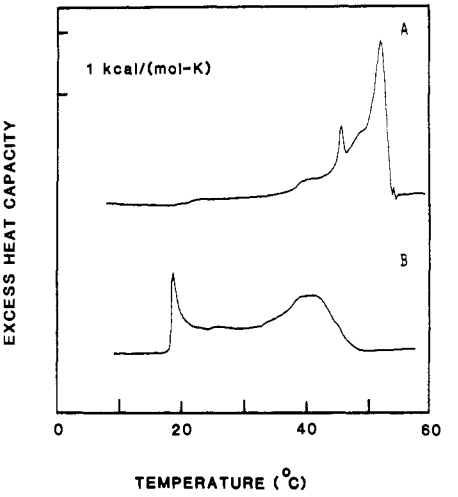

FIGURE 9: DSC profiles of mixed multilamellar bilayers of C(18)-C(18)PC–C(18)C(10)PC that contain (A) 20 mol % C(18)C(10)PC or (B) 60 mol % C(18)C(10)PC. The preparations were cooled at 5 °C/h from 60 to 0 °C and then incubated at 0 °C for 1 h prior to analysis by DSC.

CONCLUSIONS

The results obtained in this study suggest that phase separation of mixed chain length phospholipids can occur when they are mixed with symmetric chain length phospholipids in bilayers. The gel phases S_2 and S_3 represent a three-dimensional phase separation of the phospholipids within these phases; that is, the phosphatidylcholines are both laterally separated within the plane of the bilayer and conformationally coupled across the bilayer. It is possible that such laterally phase separated and coupled gel phases may occur in biological membranes. For example, a mixed interdigitated gel phase has been proposed for C(24)SPM bilayers at temperatures below 47 °C (Levin et al., 1985). Thus, in biological membranes at 37 °C a region could exist where a C(24)SPM-enriched mixed interdigitated gel phase coexists with a liquid-crystalline phase comprised of the majority of the phospholipids of the membrane. We are currently conducting experiments to investigate this possibility. Frequently, membrane components with chain length asymmetries comprise only a small fraction of the total components of the membrane. In addition, these mixed chain length components may be asymmetrically

distributed between the two leaflets of the bilayer (Rothman & Lenard, 1977). In this context, it is interesting to note that the interdigitated phase S_2 was observed when the mixed-chain phosphatidylcholine component comprised as little as 5–10 mol % of the binary mixture. The results with the C(18)C(18)-PC–C(18)C(10)PC binary mixture suggest that mixed-chain components could exhibit liquid–liquid immiscibility within biological membranes. These unique laterally separated and coupled phases could have profound implications for membrane functions. For example, interdigitation across the bilayer center of the hydrocarbon chains of membrane components with large chain length asymmetries could provide a mechanism for the transmission of information across the membrane (Schmidt et al., 1978; Nicolson, 1976). Another important property of mixed-chain membrane components could be the formation of compositional domains within membranes. For example, it has been demonstrated that asialo-GM_1 can form clustered distributions in C(14)C(14)PC liposomes (Tillack et al., 1982). Such compositional domains have been suggested to act as membrane receptors or as identifying surface structures involved in cellular recognition or cell–cell interactions. Although clustering of the neutral gangliosides could be due to intermolecular interactions within the carbohydrate region of the glycolipid, the results obtained here suggest that the mixing properties of the highly asymmetric hydrocarbon chains of the neutral gangliosides might be involved as well.

We are currently investigating the dynamic behavior of the individual components of these binary mixtures of FT-IR spectroscopy. This is being accomplished by employing chain-perdeuteriated [$^2H_{70}$]C(18)C(18)PC as the symmetric chain component. The results of this study will be reported in a future publication.

Registry No. C(18)C(18)PC, 4539-70-2; C(18)C(16)PC, 10589-48-7; C(18)C(14)PC, 17528-52-8; C(18)C(12)PC, 82181-14-4; C(18)C(10)PC, 17511-04-5.

REFERENCES

Ansell, G. B., Hawthorne, J. N., & Dawson, R. M. C. (1973) in *Form and Function of Phospholipids*, Elsevier, New York.

Blume, A., Wittebort, R. J., & Das Gupta, S. K. (1982) *Biochemistry 21*, 6243.

Boggs, J. M., Stamp, D., & Mascarello, M. A. (1981) *Biochemistry 20*, 6066.

Chen, S. C., & Sturtevant, J. M. (1981) *Biochemistry 20*, 713.

Curatolo, W., Sears, B., & Neuringer, L. J. (1985) *Biochim. Biophys. Acta 817*, 261.

Findlay, E. J., & Barton, P. G. (1978) *Biochemistry 17*, 2400.

Gomori, G. (1942) *J. Lab. Clin. Med. 27*, 955.

Huang, C., & Mason, J. T. (1986) *Biochim. Biophys. Acta 864*, 423.

Huang, C., Mason, J. T., & Levin, I. W. (1983) *Biochemistry 22*, 2775.

Hui, S. W., Mason, J. T., & Huang, C. (1984) *Biochemistry 23*, 5570.

Jacobs, R. E., Hudson, B. S., & Anderson, H. C. (1977) *Biochemistry 16*, 4349.

Jaworsky, M., & Mendelsohn, R. (1985) *Biochemistry 24*, 3422.

Knoll, W., Ibel, K., & Sackman, E. (1981) *Biochemistry 20*, 6379.

Lee, A. G. (1977) *Biochim. Biophys. Acta 472*, 285.

Levin, I. W., Thompson, T. E., Barenholz, Y., & Huang, C. (1985) *Biochemistry 24*, 6282.

Luna, E. J., & McConnell, H. M. (1978) *Biochim. Biophys. Acta 509*, 462.

Mabrey, S., & Sturtevant, J. M. (1976) *Proc. Natl. Acad. Sci. U.S.A. 73*, 3862.

Mason, J. T., Broccoli, A. V., & Huang, C. (1981a) *Anal. Biochem. 113*, 96.

Mason, J. T., Huang, C., & Biltonen, R. L. (1981b) *Biochemistry 20*, 6086.

Mason, J. T., Huang, C., & Biltonen, R. L. (1983) *Biochemistry 22*, 1013.

Matubayasi, N., Shigematsu, T., Ichara, T., Kamaya, H., & Ucda, I. (1986) *J. Membr. Biol. 90*, 37.

McIntosh, T. J., Simon, S. A., Ellington, J. C., & Porter, N. A. (1984) *Biochemistry 23*, 4038.

Mendelsohn, R., & Maisano, J. (1978) *Biochim. Biophys. Acta 506*, 192.

Nicolson, G. L. (1976) *Biochim. Biophys. Acta 457*, 57.

Priest, R. (1980) *Mol. Cryst. Liq. Cryst. 60*, 167.

Rothman, J. E., & Lenard, J. (1977) *Science (Washington, D.C.) 195*, 743.

Schmidt, C. F., Barenholz, Y., Huang, C., & Thompson, T. E. (1978) *Nature (London) 271*, 775.

Schmidt, G., & Knoll, W. (1986) *Chem. Phys. Lipids 39*, 329.

Serrallach, E. N., deHaas, G. H., & Shipley, G. G. (1984) *Biochemistry 23*, 713.

Shimshick, E. J., & McConnell, H. M. (1973) *Biochemistry 12*, 2351.

Silvius, J. R. (1986) *Biochim. Biophys. Acta 857*, 217.

Silvius, J. R., & Gagné, J. (1984a) *Biochemistry 23*, 3232.

Silvius, J. R., & Gagné, J. (1984b) *Biochemistry 23*, 3241.

Simon, S. A., & McIntosh, T. J. (1984) *Biochim. Biophys. Acta 773*, 169.

Small, D. M. (1984) *J. Lipid Res. 25*, 1490.

Stümpel, J., Ebil, H., & Nicksch, A. (1983) *Biochim. Biophys. Acta 727*, 246.

Sugar, I. P., & Monticelli, G. (1985) *Biophys. J. 48*, 283.

Tillack, T. W., Wong, M., Alietta, M., & Thompson, T. E. (1982) *Biochim. Biophys. Acta 691*, 261.

vanDijck, P. W. M., Kaper, A. J., Oonk, H. A. J., & deGier, J. (1977) *Biochim. Biophys. Acta 470*, 58.

Wilkinson, D. A., & Nagle, J. F. (1979) *Biochemistry 18*, 4244.

Wu, S. H., & McConnell, H. M. (1975) *Biochemistry 14*, 847.